EE213. Microscopic Nanocharacterization of Materials
Lecture 13. 2016

Three Dimensional Imaging/Characterization

Holography
Tomography

March 1, final paper rough outline due. COB

Final Paper

1. Paper: due last day of class

2. Topic should be about a particular microcharacterization technique and comparison with at least one other method. From topics covered in course outline.

3. You must discuss the spatial resolution characteristics and limits.

4. Abstract or summary of each paper listed as references.

5. Discuss typical application use, briefly.

EE213. Final Topics

Ryan Gardner	Photoelectron microscopy
M. Ahsan Habib	NSOM
Bingzhang Lu	Atomic Force Microscopy
Evan Petersen	Confocal, 2 photon and wide field microscopy
Renee Sully	SIMS
Bin Yao	?

HOLOGRAPHY principle

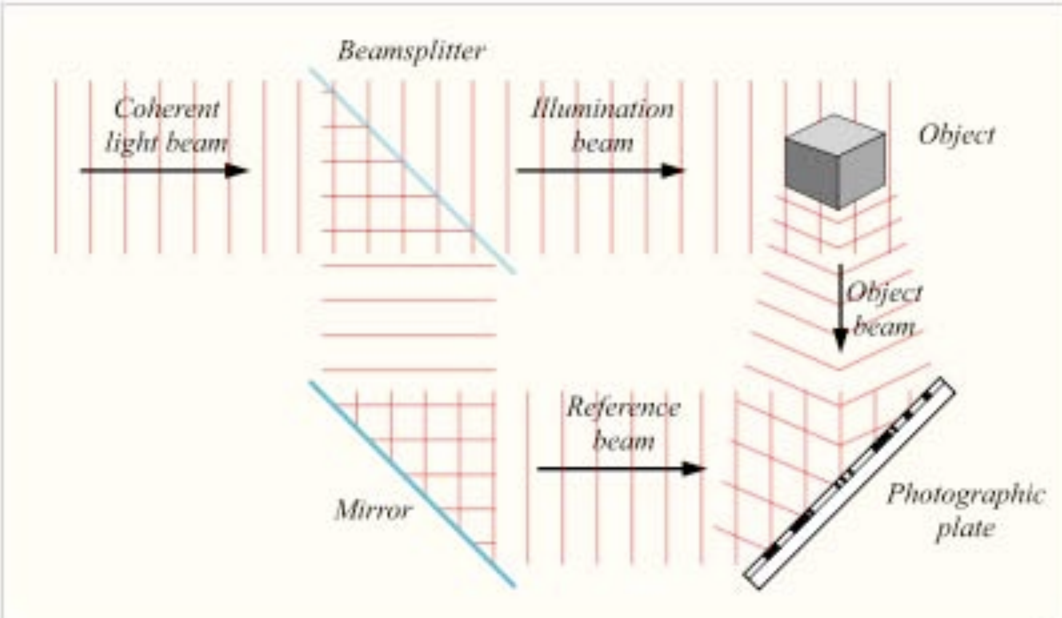

Recording a hologram

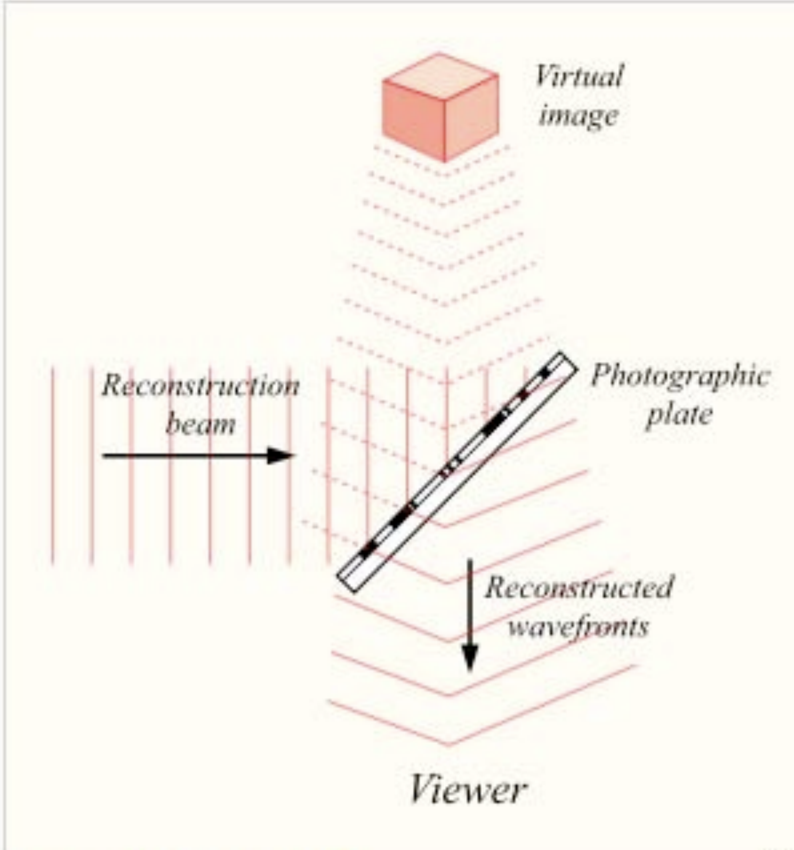

Reconstructing a hologram

From Wikipedia

Photographed Images at 2 different angles from a hologram of a mouse

electron holography – another characterization tool.

original idea by Gabor in the ~~1950's~~ 1940's /
D. Gabor (1948). Nature. 161. ~~563-564~~ 777-778. / 1949 Proc. Roy. Soc (Lon). 197. (1051) 454-487

idea was to correct the aberrations of electron microscope lenses —

Nobel Prize in the '70s / 1971

demonstrated with lasers in the ~~late~~ early '60's — (Leith & Upatnieks. JOSA. 52. 1123-30)

and with electrons in the '80's —

basically creating an interference pattern that has info on amplitude and phase of scattered wave
– a single image only contains the amplitude info since it is $I(x,y) = |Ae^{i\varphi}|^2$ ←

holography was an alternative to aberration correction AND it allowed one to create a 3D image \\

most useful in mapping $\vec{E}$ and $\vec{B}$ fields since they change the "phase" of an electron wave.

exception of Rothamsted Experimental Station and a few centres in the United States, there existed no other laboratory where experience in so many aspects of plant virus study could be obtained, applications from foreign workers for this training became very frequent. Unfortunately, these activities had to be severely curtailed owing to the lack of laboratory accommodation. Nevertheless, it may be mentioned that students have come to take either research degrees or courses of instruction in plant virus work from Argentina, Australia, Belgium, Brazil, Canada, China, Czechoslovakia, Denmark, Gold Coast, India, New Zealand, Poland, Portugal, South Africa, Sweden and the United States, and visitors have come from all over the world.

In looking back over two decades, it becomes evident how, with increasing knowledge and new technical discoveries, the trend of virus research has changed. In the beginning, most of the emphasis was placed on the disease, and symptomatology was all-important, although the study of the relationships between the viruses and their insect vectors was already being undertaken. The isolation of tobacco mosaic virus by Stanley in 1935, however, was the key which opened the door to the study of the virus itself, quite apart from the disease it may cause. A brief review of some of the main contributions by the Cambridge workers illustrates this change of emphasis in virus research. For the first few years, attention was directed almost entirely towards potato virus diseases, and from this work three items of interest may be noted. The first of these was the identification of the insect vector of potato leaf-roll, which was later also found to carry another potato virus. This was the aphis, *Myzus persicæ*, and it was almost the first introduction to public notice of the aphis which, since that time, has become of paramount importance in the field of plant viruses and seems to be the most efficient vector of these agents in the world. It is now known to transmit more than twenty distinct viruses. The next addition to our knowledge of potato viruses was the discovery of the paracrinkle virus in potatoes of the variety King Edward; this is one of the unsolved puzzles of the virus world, since it is present in all plants of this potato variety, but no method is known by which it can spread in Nature. The case of paracrinkle is often quoted as evidence of the heterogenesis of viruses by those who hold this view. The third item was the analysis, for the first time, of a plant virus complex by differential methods of transmission, and the isolation of the two potato viruses now universally known as X and Y.

In 1931 the virus of tomato spotted wilt was discovered for the first time in Europe; it was found in an ornamental plant sent to Cambridge from Cardiff. Before this it had not been seen outside Australia. Since then the distribution of the virus has become world-wide, and in Great Britain it is one of the major problems of the tomato grower with 'mixed houses'.

The viruses of tomato bushy stunt and tobacco necrosis, both described for the first time in Cambridge, have proved of great scientific interest. The virus of tomato bushy stunt, about which more is known than of most viruses, was the first to be isolated in a three-dimensional crystalline form, and this was accomplished by Bawden and Pirie, after the former had left Cambridge. Shortly after this the virus of tobacco necrosis was isolated as thin crystalline plates. About this time, also, the comparatively new technique of plant virus serology was applied to the study of potato virus X.

In 1938 a new virus complex affecting the tobacco plant, known as 'rosette', was investigated, the chief point of interest being the apparent relationship between the two component viruses. This is suggested by the fact that, while both viruses are aphis-transmitted if they are together in the plant, one of the two cannot be picked up by the insect if the other virus is not present.

During the period 1940–45, several new viruses have been described, those of *Arabis*, *belladonna* and lovage mosaic, tobacco broken ringspot, tomato black ring and of two new potato diseases, veinal necrosis and veinal yellows, which were found in some South American potatoes. Of these new viruses, those of *Arabis* mosaic and broken ringspot are of especial interest, since they appeared in plants inside the experimental glasshouses with no apparent explanation of their origin.

During the last two years an extremely interesting and important new virus has been discovered and studied. Known as turnip yellow mosaic virus, it has been isolated in two different crystalline forms and, like other plant viruses studied so far, it is a nucleoprotein. In addition to the active virus, infected plants also contain a protein which is apparently the virus protein but lacks the nucleic acid. This protein has also been crystallized, and studies of the biological and biophysical properties of these two proteins are now in progress. The virus is also of interest in having an entirely new kind of insect vector, one with biting mouthparts, namely, a flea-beetle. This is the first record, both of transmission of a virus by this insect and of the insect transmission of a crystalline plant virus.

Electron microscope studies in conjunction with Dr. V. E. Cosslett of the Cavendish Laboratory, and with Dr. R. W. G. Wyckoff in the United States, have also been made [see p. 760 of this issue of *Nature*]. An interesting outcome of this work is that the structure of the crystals of tobacco necrosis virus and turnip yellow mosaic virus has been demonstrated by this means.

A NEW MICROSCOPIC PRINCIPLE

By Dr. D. GABOR
Research Laboratory, British Thomson-Houston Co., Ltd., Rugby

It is known that the spherical aberration of electron lenses sets a limit to the resolving power of electron microscopes at about 5 A. Suggestions for the correction of objectives have been made; but these are difficult in themselves, and the prospects of improvement are further aggravated by the fact that the resolution limit is proportional to the fourth root of the spherical aberration. Thus an improvement of the resolution by one decimal would require a correction of the objective to four decimals, a practically hopeless task.

The new microscopic principle described below offers a way around this difficulty, as it allows one to dispense altogether with electron objectives. Micrographs are obtained in a two-step process, by electronic analysis, followed by optical synthesis, as in Sir Lawrence Bragg's 'X-ray microscope'. But

A NEW MICROSCOPIC PRINCIPLE

By Dr. D. GABOR
Research Laboratory, British Thomson-Houston Co., Ltd., Rugby

IT is known that the spherical aberration of electron lenses sets a limit to the resolving power of electron microscopes at about 5 A. Suggestions for the correction of objectives have been made; but these are difficult in themselves, and the prospects of improvement are further aggravated by the fact that the resolution limit is proportional to the fourth root of the spherical aberration. Thus an improvement of the resolution by one decimal would require a correction of the objective to four decimals, a practically hopeless task.

The new microscopic principle described below offers a way around this difficulty, as it allows one to dispense altogether with electron objectives. Micrographs are obtained in a two-step process, by electronic analysis, followed by optical synthesis, as in Sir Lawrence Bragg's 'X-ray microscope'. But

A NEW MICROSCOPIC PRINCIPLE

By Dr. D. GABOR
Research Laboratory, British Thomson-Houston Co., Ltd., Rugby

IT is known that the spherical aberration of electron lenses sets a limit to the resolving power of electron microscopes at about 5 A. Suggestions for the correction of objectives have been made; but these are difficult in themselves, and the prospects of improvement are further aggravated by the fact that the resolution limit is proportional to the fourth root of the spherical aberration. Thus an improvement of the resolution by one decimal would require a correction of the objective to four decimals, a practically hopeless task.

The new microscopic principle described below offers a way around this difficulty, as it allows one to dispense altogether with electron objectives. Micrographs are obtained in a two-step process, by electronic analysis, followed by optical synthesis, as in Sir Lawrence Bragg's 'X-ray microscope'. But

The principle of wave-front reconstruction

Consider a coherent monochromatic wave with a complex amplitude U striking a photographic plate. We write $U = Ae^{i\psi}$, where A and ψ are real. U may be decomposed into a 'background wave' $U_0 = A_0e^{i\psi_0}$, and a remainder $U_1 = A_1e^{i\psi_1}$ which is due to the disturbance created by the object and may be called the secondary wave. Thus the complex amplitude at the photographic plate is

$$U = U_0 + U_1 = A_0e^{i\psi_0} + A_1e^{i\psi_1} = e^{i\psi_0}(A_0 + A_1e^{i(\psi_1-\psi_0)}) \tag{1}$$

and its absolute value $A = [A_0^2 + A_1^2 + 2A_0A_1 \cos(\psi_1 - \psi_0)]^{\frac{1}{2}}$.

from Gabor, 1949

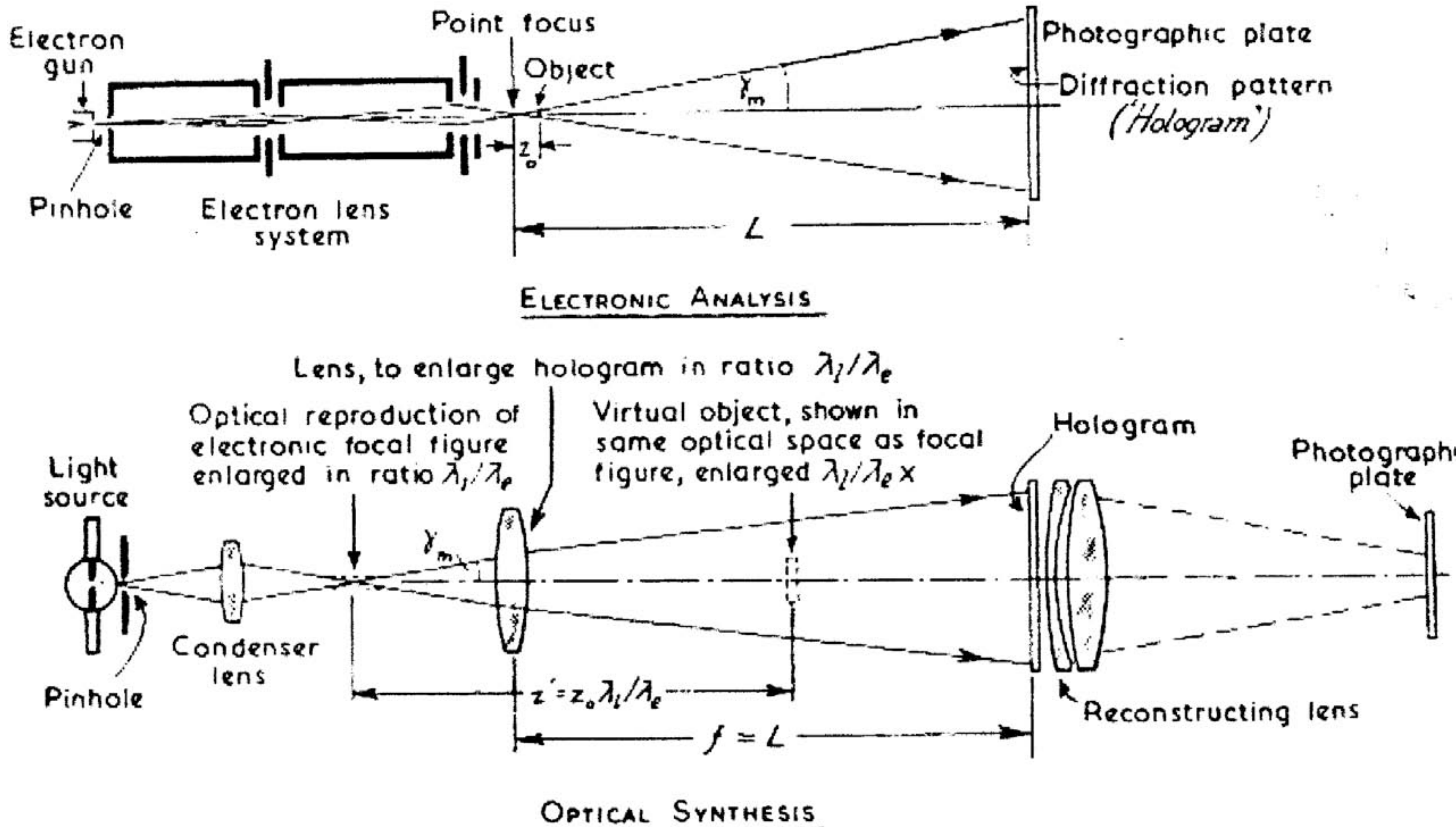

FIGURE 1. Principle of electron microscopy by reconstructed wave-fronts.

from Gabor, 1949.

HOLOGRAPHY principle

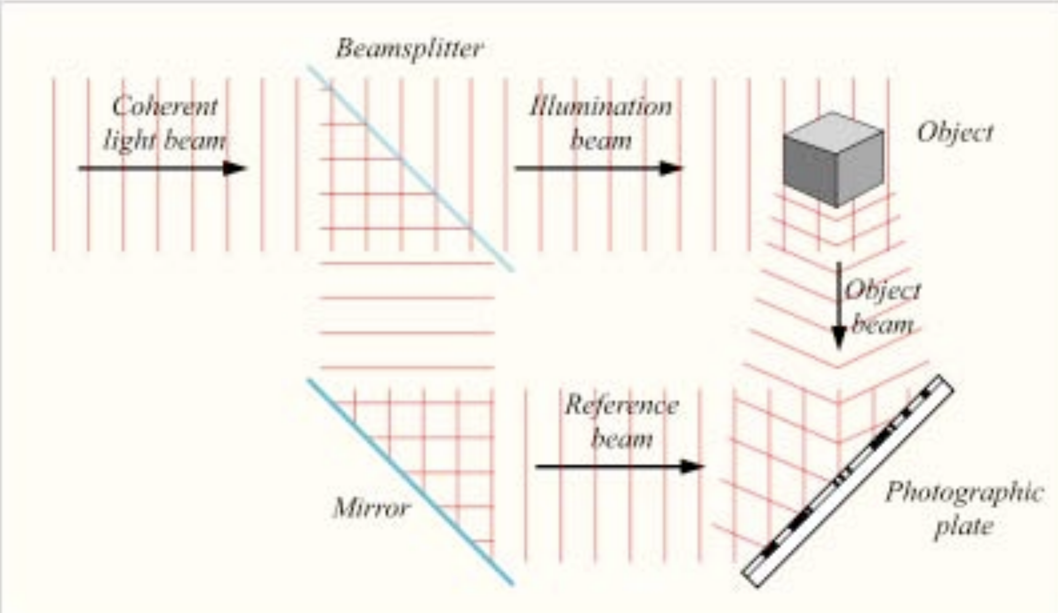

Recording a hologram

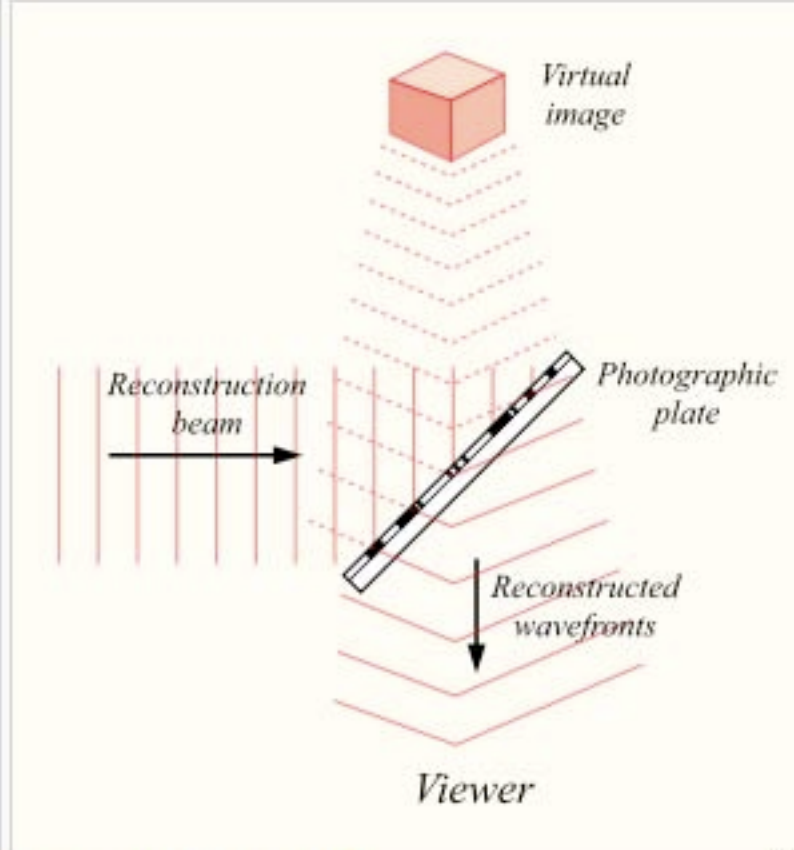

Reconstructing a hologram

From Wikipedia

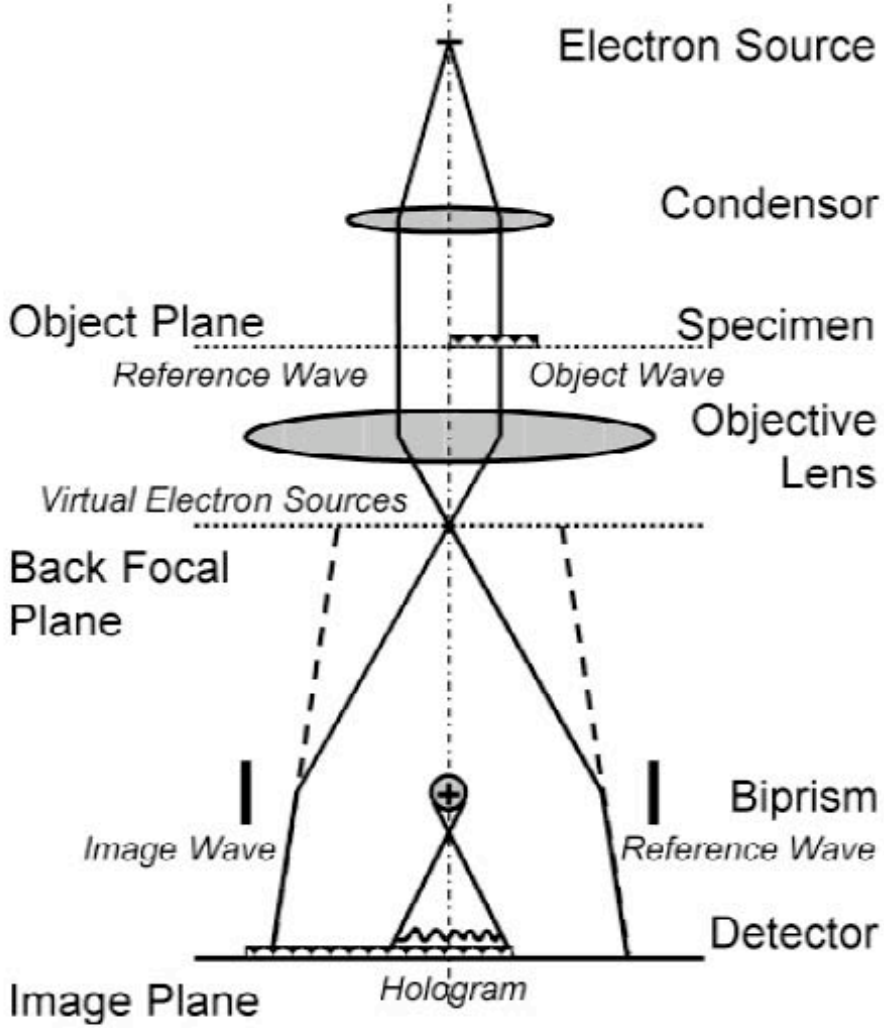

Lehmann and Lichte. Microscopy and Microanalysis. 8(6).447-466. (2002)

Figure 6. Taking a hologram. The object under investigation covers only half of the object plane, whereas the other half serves as a reference area. The reference wave as well as the object wave are imaged by the objective lens. Due to the wave transfer function, the object wave is changed so that the aberrated image wave is formed. The biprism deflects both parts of the wave towards each other, yielding the hologram in the overlapping region.

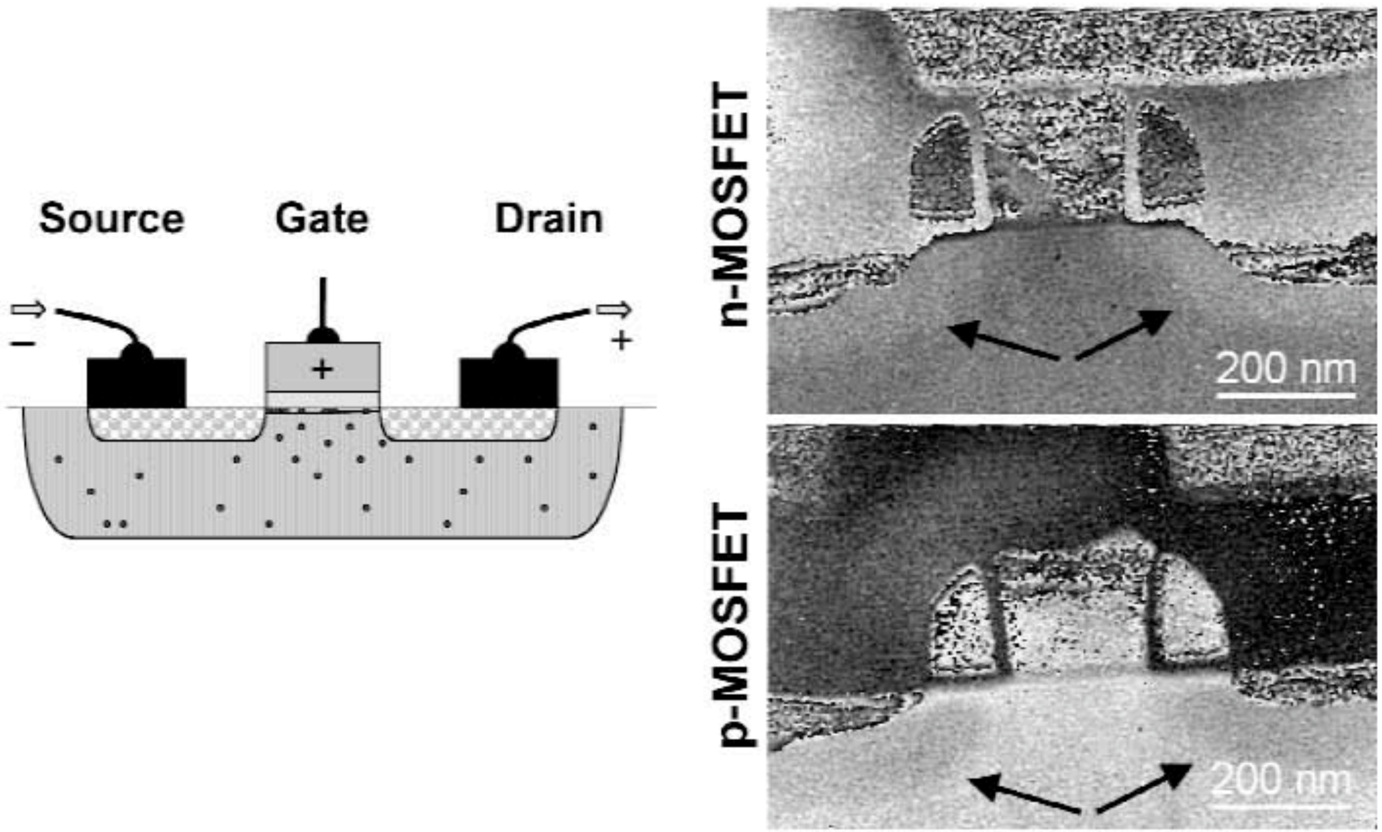

Figure 16. Dopant profiling. The alignment of the dopants with respect to the gate electrode is increasingly critical with increasing integration density. Holographic phase images allow the mapping of potential distribution arising due to doping. The dark and bright seam (arrows) shows the potential distribution with opposite sign in p-doped and n-doped MOSFETs, respectively.

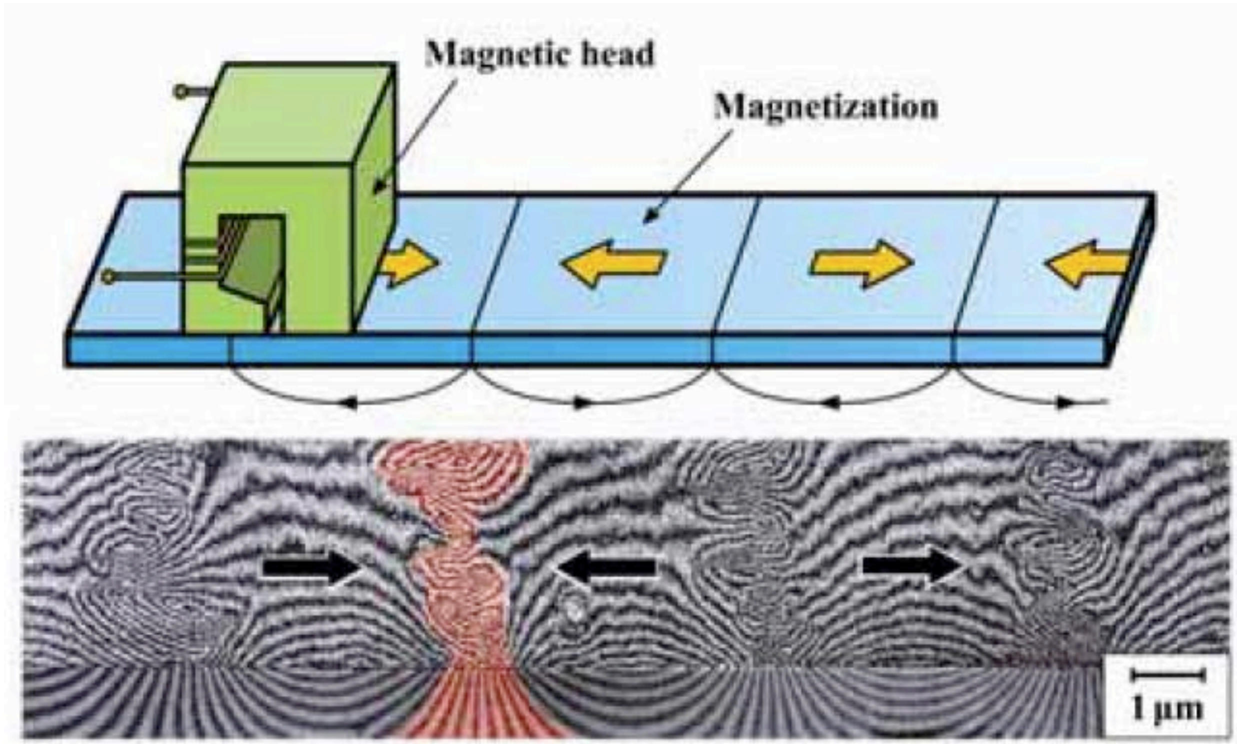

Fig. 9. Magnetic lines inside and outside a recorded magnetic tape. Detailed magnetic lines observed under various conditions, such as tape material and spacing and gap of head, provide information about how higher density recording can be attained.

From Tonomura,

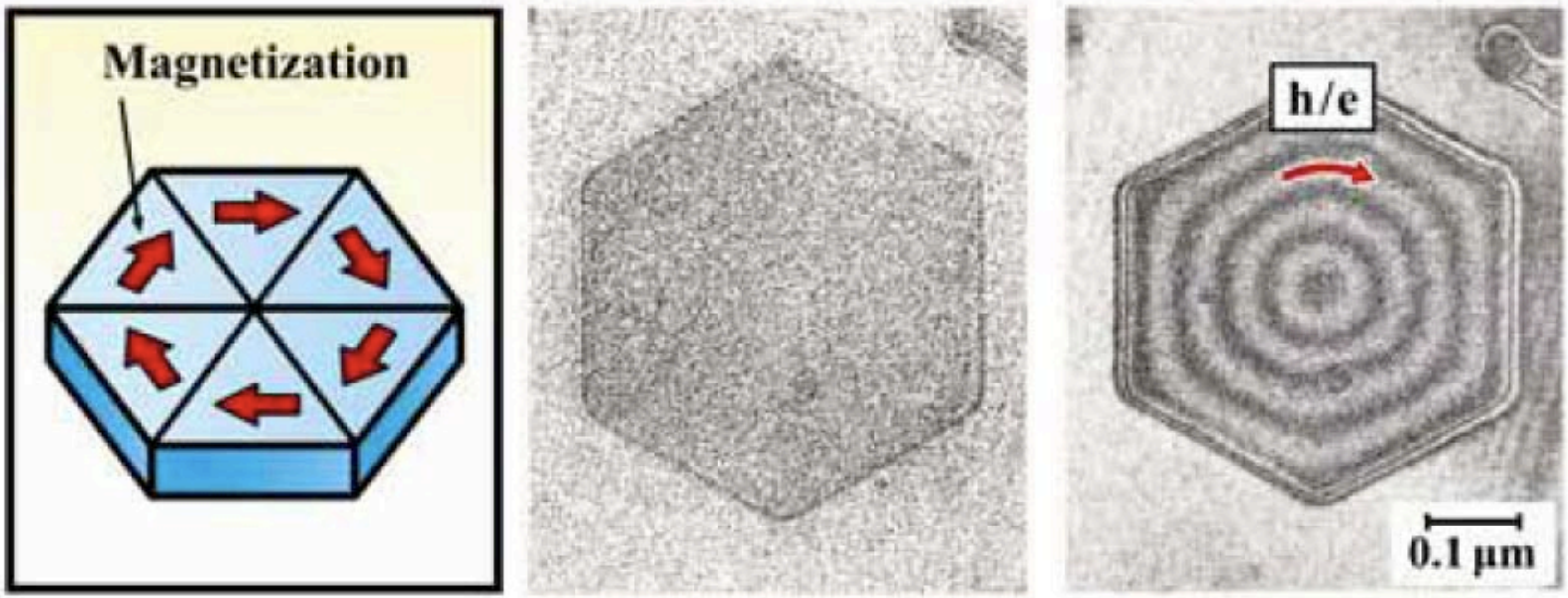

(a) (b) (c)

Fig. 6. Hexagonal cobalt particle. (a) Schematic. (b) Electron micrograph. (c) Interference micrograph (phase amplification × 2). Phase contours in interference micrograph (c) indicate magnetic lines in $h/2e$ flux units. Magnetic lines are circular inside the particle.

From Tonomura,

Electron Holography: mapping electric fields

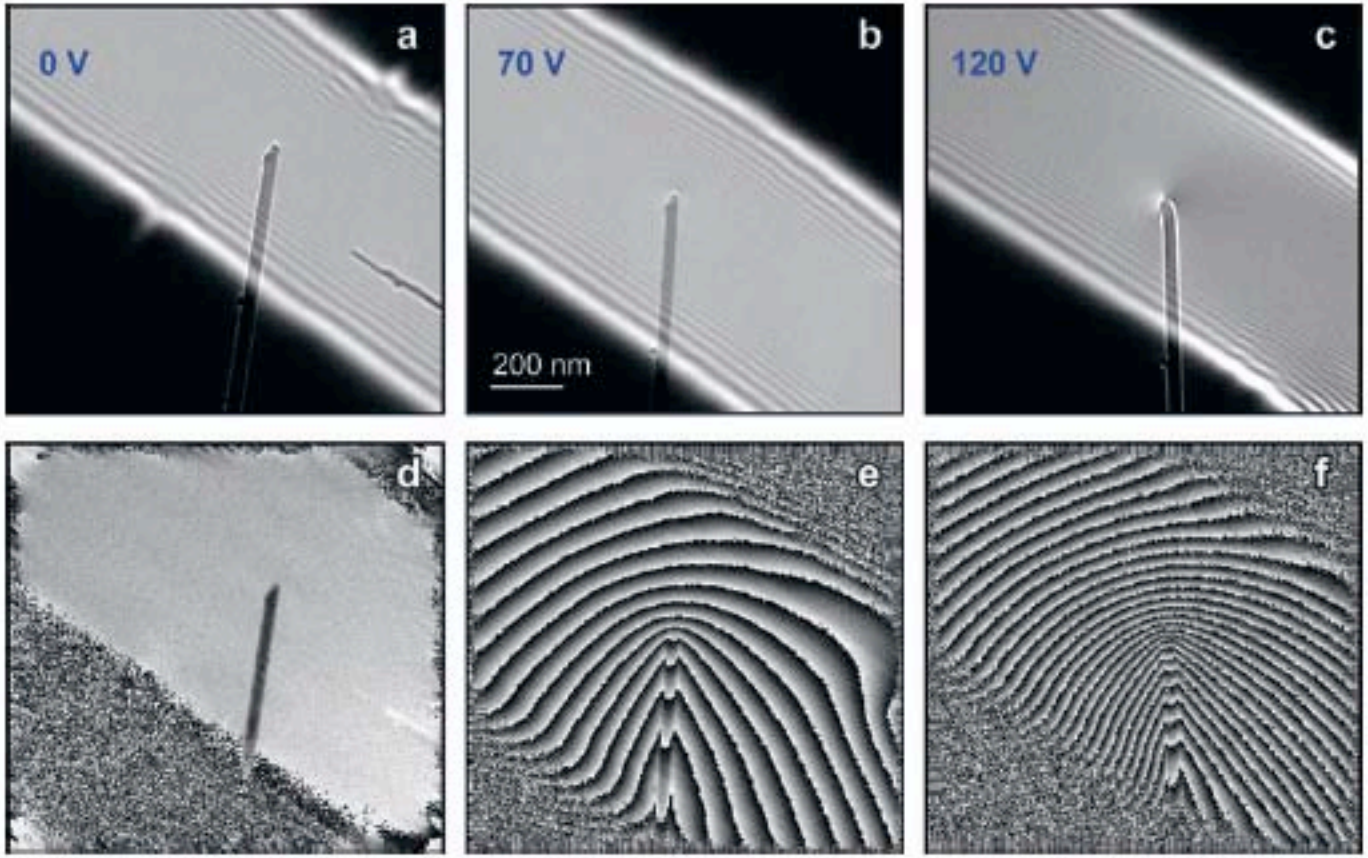

Figure 8

Observation of a field-emitting carbon nanotube. *a*, *b*, and *c* show electron holograms at bias voltages $V_B = 0$ V, 70 V, and 120 V, respectively. *d*, *e*, and *f* show reconstructed phase images corresponding to *a*, *b*, and *c*, respectively. The phase contours correspond to a spacing of 2π radians. The phase gradient in *f* corresponds to an electric-field strength of ~ 1.2 V nm^{-1} at the tip of the nanotube (from Reference 89).

tomography / 3D imaging.

holography was one method of getting "3D".

tomography uses method of reconstructed 2D projections.
ie, one needs a series of "[redacted] projection" images
taken from different directions.

one does this in either Fourier space or Real space. //

1st paper that performed this "reconstruction" in 1968
DeRosier and Klug. (1968). Nature. 217. [redacted] 130-134.
used Fourier proj. reconstr.
- this works best for periodic objects.

show their cartoons of FT projections

another method that is widely used, particularly
for objects which may not have periodicity (or symmetry)
is the "back projection" method.
based on the Radon transformation (rather than Fourier)
Johann Radon (1917).
translated in 1986 → [redacted]
P.C. Parks (1986). IEEE Transactions on Medical Imaging. Vol. MI-5. (4). 170-176.

Radon transform ⟹ sinogram

Tomography

Tomography used in all radiation characterization methods.

example:

x ray absorption µscopy.

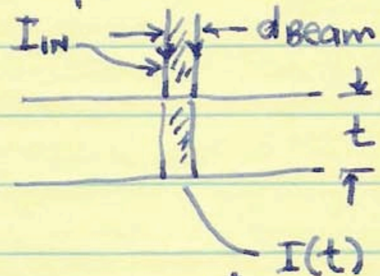

$$I_{IN} \rightarrow \quad \frac{I(t)}{I(0)} = e^{-\int_0^t (\mu/\rho)\rho t}$$

the line integral of absorption over the thickness (slice)

∴ you get a "projected" density map through the sample for each "view" —

The Radon transform

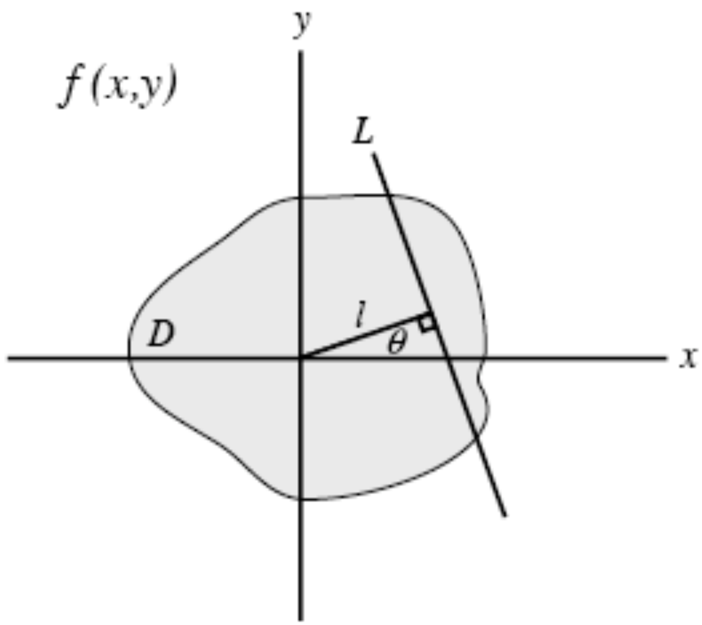

Fig. 1. The Radon transform R can be visualised as the integration through a body D in real space $f(x, y)$ along all possible line integrals L, with its normal at an angle θ to the horizontal.

Radon transform / $Rf(\ell,\theta) = \int_L f(x,y)\,ds$

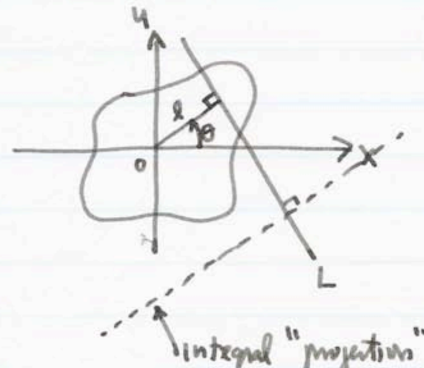

take series of projections thru object
at diff θ (for various ℓ).

then "back-project" (inverse transform) to reconstruct original //
⟶ back projection

note that the more projections you use, the closer you get
to original object // (same is true for Fourier space projections)

this means one needs many "images" to reconstruct 3d object
but once you have the 3d, you can then go back and
look at any slice ///

good reviews /

biol / R. McIntosh, D. Nicastro and D. Mastronarde.
Trends in Cell Biology. 15(1). 2006. 43–51.

materials / P.A. Midgley & M. Weyland. Ultramicroscopy. 96 (2003) 413–431.

How Back Projection Works (simplified)

take a 2×2 pixel tomogram

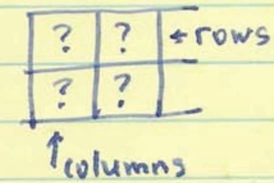

take two tilt projections / at 90° to each other

we measure $\int f(x)dx$ across the rows or columns

example:

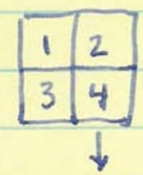

→ $\int f(x)dx = 1+2 = 3$

↓ $\int f(x)dx = 2+4 = 6$

so we can measure the "sum" of intensities across each "tilt" direction – in this case, over the rows or columns.

the trick is to find out how those intensities are distributed.

Back Projection (cont)

row sums ← we measure this

		row sums
?	?	7
?	?	11
8	10	////

column sums

↗ we measure this

step 1. back project.

- guess intensities equally distributed
- do it 1st over the rows

∴ 1st guess: $\frac{\text{initial row sum}}{\#\text{pixels summed}}$ | $\frac{7}{2} = 3.5$, $11/2 = 5.5$

		row sum
3.5	3.5	3.5+3.5 = 7 ("7")
5.5	5.5	5.5+5.5 = 11 ("11")

column sum

("7"), ("11") — measured

└ note: column sums now not original measured sums.

step 2. back project

- do the same for column sums.

ie, $\frac{\text{initial column sum}}{\#\text{pixels summed}}$ | $\frac{8}{2} = 4$, $\frac{10}{2} = 5$

add to 1st guess

Back Projection (cont)

step 2. (cont)

from step 1

			rowsum
	3.5 +4.0	3.5 +5.0	("7")
	5.5 +4.0	5.5 +5.0	("11")
column sum	("8")	("10")	

original values (row sums); original values (column sums)

step 3. add up each row, column
subtract that from original (measured) sums.

			row sum (new)
	7.5	8.5	7 - 16 = -9
	9.5	10.5	11 - 20 = -9
column sum	("8")	("10")	

original values

step 4. divide new row sum by # pixels
ie, -9/2 = -4.5
and add this to our "guess"

			row sum
	7.5 -4.5	8.5 -4.5	
	9.5 -4.5	10.5 -4.5	
column sum			

3	4
5	6

next guess at the elements

step 5. now add densities of each column
and subtract from original column sum (8, 10)

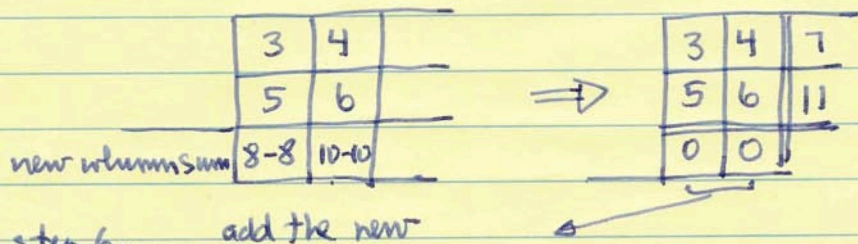

step 6. add the new
column sum
divided by # pixels to the row sum

$\therefore \frac{0}{2} = 0$ etc.

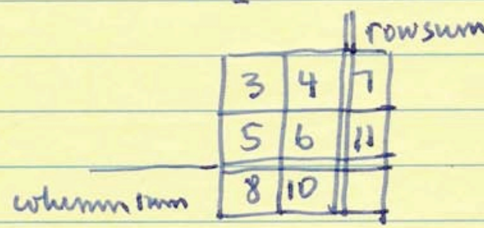

these sums match
the original,
$\therefore$ the iteration stops
reconstruction is complete!

In a typical EM or optical tomogram
there would be 50-100 projections each with
1/4 - 1 M pixels or more.
$\therefore$ a tomogram would contain $> 10^8$ pixels!

Tomography

Tomography used in all radiation characterization methods.

example:

x ray absorption microscopy.

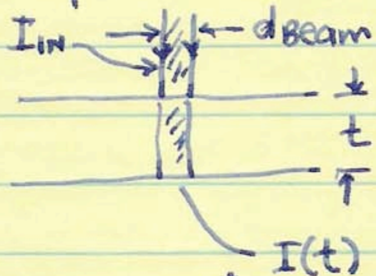

$$I_{IN} \rightarrow \frac{I(t)}{I(0)} = e^{-\int_0^t (\mu/\rho)\rho t}$$

the line integral of absorption over the thickness (slice)

∴ you get a "projected" density map through the sample for each "view" —

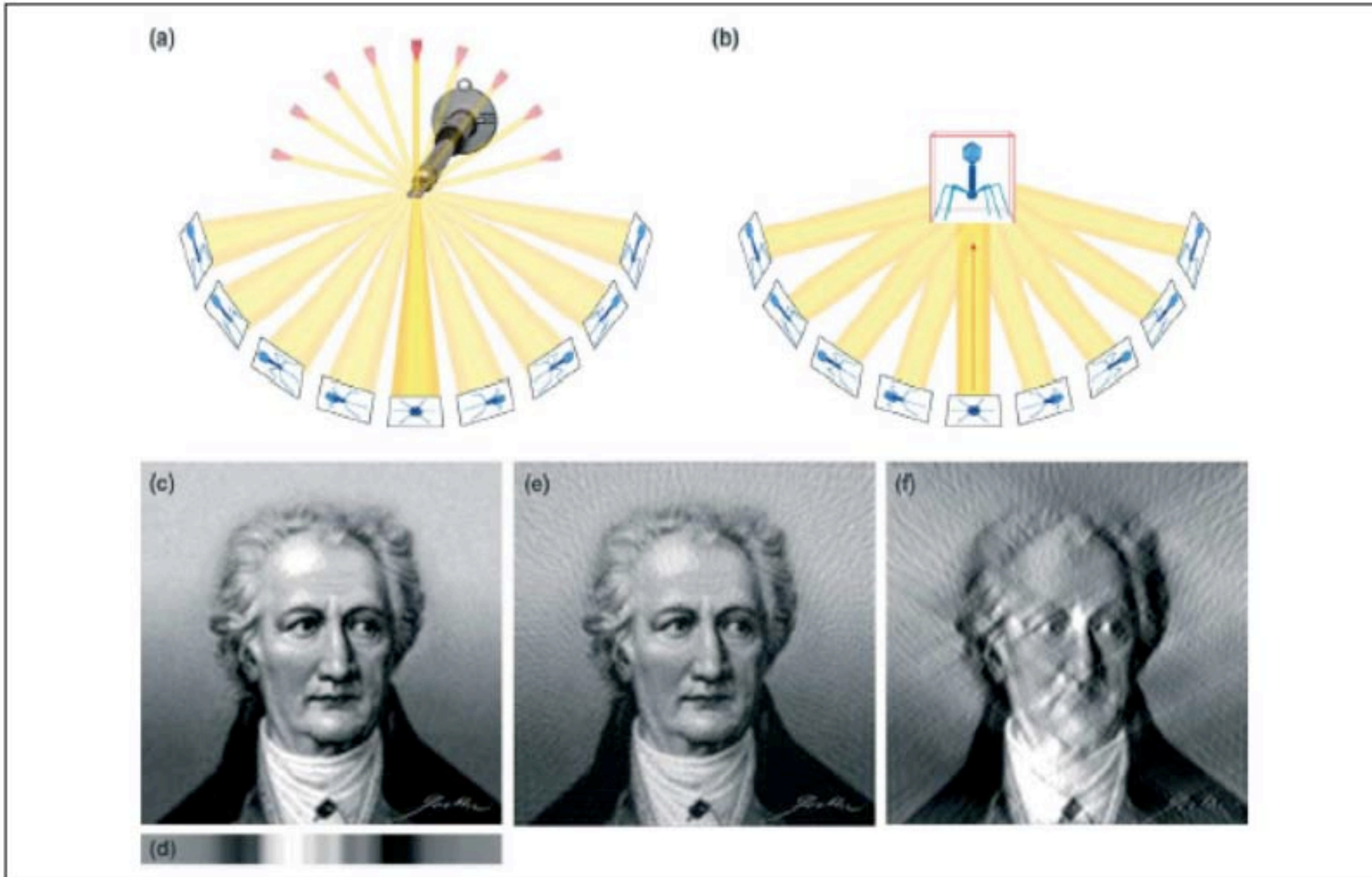

Figure 1. Principles of ET. **(a)** A biological specimen, in this case a bacteriophage contained in an EM sample holder, can be imaged from several orientations by tilting the holder in the microscope. **(b)** Process of computed back-projection, in which each tilted view is used to contribute to a reconstruction of the original structure. **(c)** Example of a 2D image (the face of Goethe), representing a slice cut from a 3D object in a plane perpendicular to the tilt axis. **(d)** Projection of the 2D object as a 1D distribution of densities reflecting the summation of all of the brightness in the picture along a set of vertical lines. **(e)** Reconstruction of Goethe's face achieved by back-projecting 90 of the 1D projections taken at 2° intervals between +90° and −90° from the horizontal. The ripples in the image represent the resolution limitation caused by having only 90 images. Twice the number of images taken at half the tilt increment would reduce the size of the ripples by approximately twofold. **(f)** A further limitation on resolution is imposed by reconstructing the image from a more restricted range of tilted views taken between +60° and −60° from the horizontal. Because a wedge of data is missing, the reconstruction quality is anisotropically degraded. The vertical detail is still sharp (note the clarity of the shoulders, the nose and the ear); by contrast, the horizontal detail is poorly defined (note the virtual absence of a mouth). This kind of anisotropy is characteristic of single-axis tomograms constructed from data collected from a limited range of tilt.

Goethe Projections

R.McIntosh,et.al. 2005

- Demonstration of the FBP algorithm:

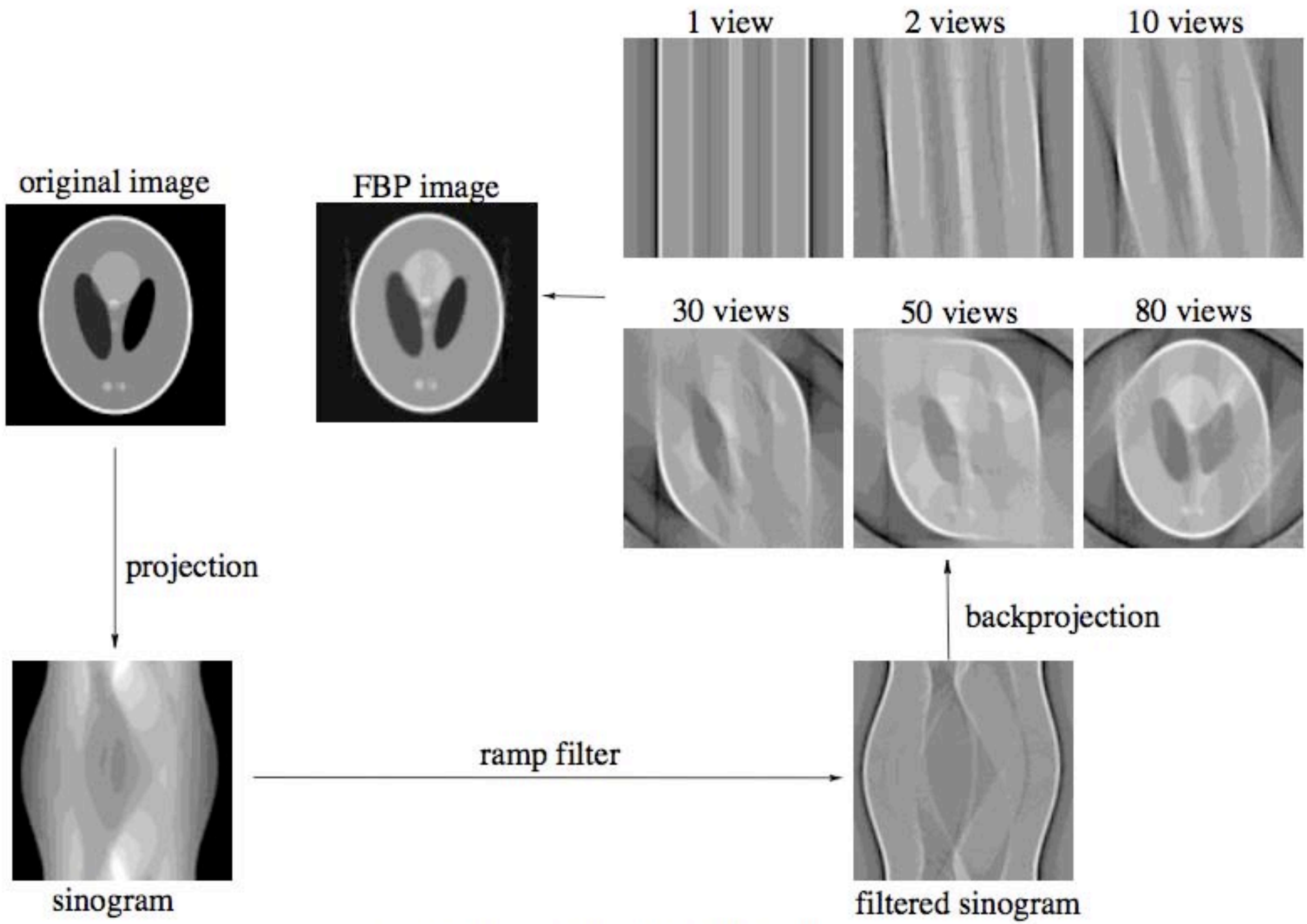

Figure 8. Demonstration of the FBP algorithm.

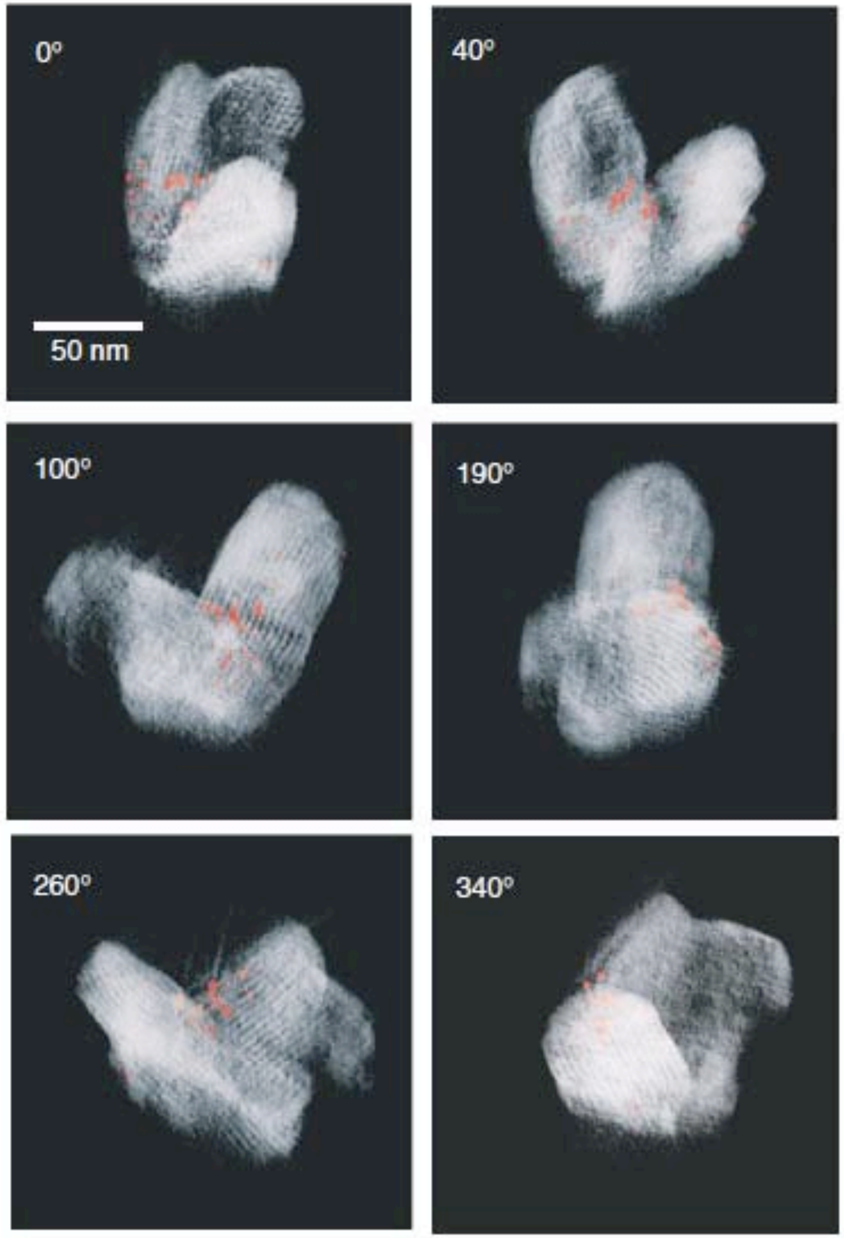

Midgley and Weyland.
Ultramicroscopy. 96(2003).413-431.

Fig. 8. (a) A montage in which each image is a voxel projection of the 3D reconstruction of an MCM41-Pd_6Ru_6 catalyst viewed at angles shown in the figure. The 3D structure of the mesopores is well resolved. The nanoparticles are coloured red to improve clarity.

MC41-Pd_6Ru_6 catalyst (HAADF signal)

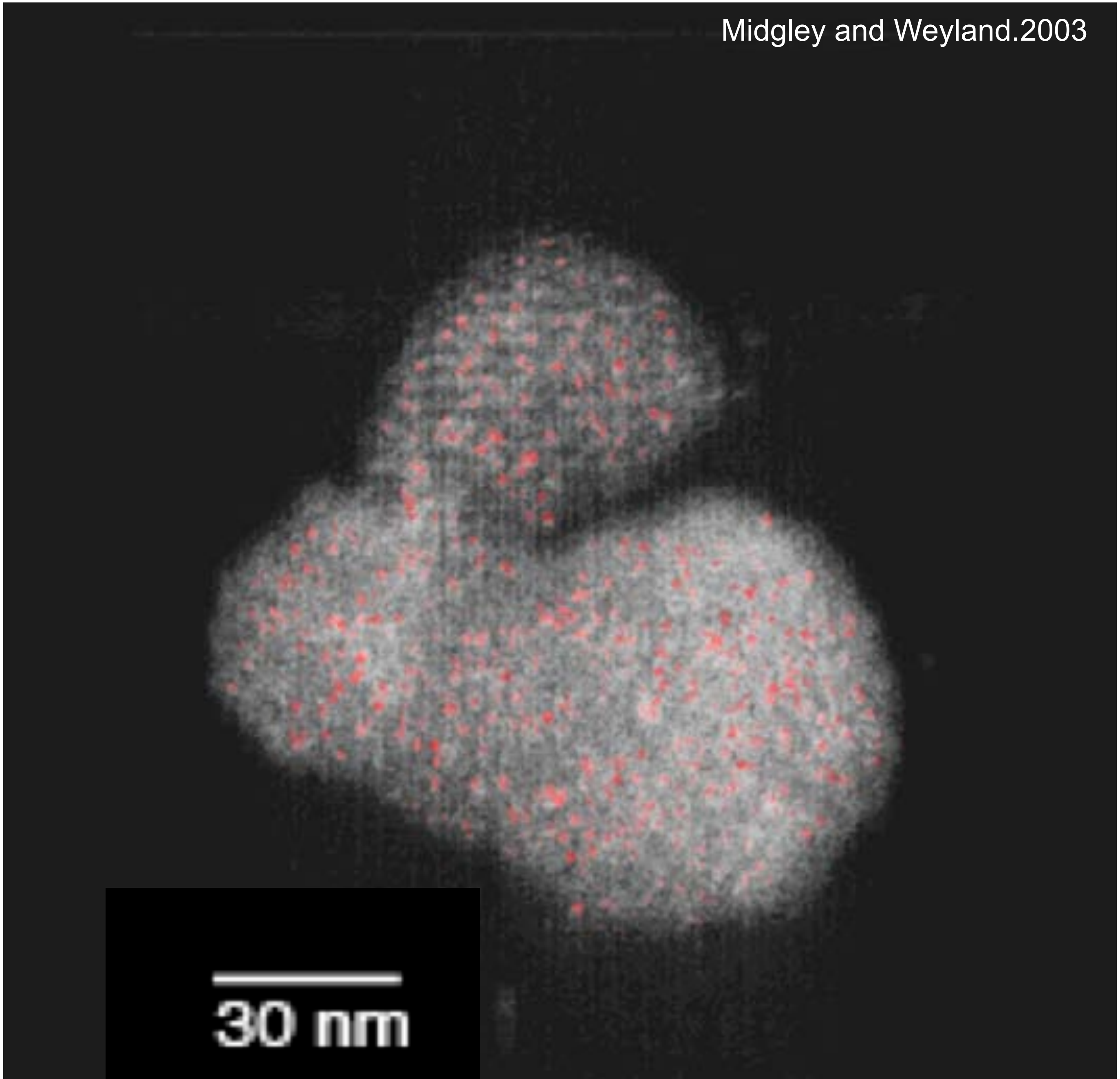

Some references

Tomography:

R. McIntosh et.al. (2005). Trends in Cell Biology. 15(1).pp.43-61.

P.A. Midgley and M. Weyland. Ultramicroscopy. 96(2003). pp. 413-431

General: Steven W. Smith. The Scientists and Engineers Guide to Digital Image Processing. www.dspguide.com can download for free

Holography:

D. Gabor. Nature. 161.(1948).pp. 777-778.
Leith and Upatnicks. JOSA. 52.pp 1123-1130.

H. Lichte and M. Lehmann. Rept.Prog. Phys.71 (2008)016102.

A. Tonomura. Electron Holography. In Springer Series in Optical Sciences.70. (1999).pp 29-49.

What are the Limits in Determining Three Dimensional Structure By Electron Microscopy?

Radiation damage due to the large number of exposures needed "damage" due to electron collisions. //

1. "elastic"
pure kinematics

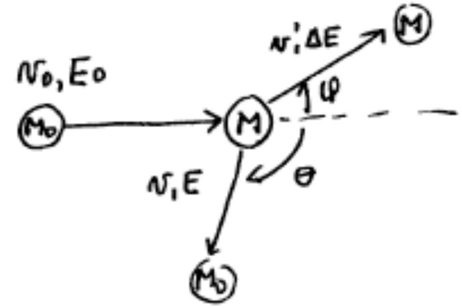

from before /

$$\frac{E}{E_0} = K = \left[\frac{x\cos\theta + \sqrt{1 - x^2 \sin^2\theta}}{1+x} \right]^2, \quad x = \frac{M_0}{M} = \frac{m_e}{Am_p}$$

when $M_0 = m_e$, $M = Am_p$ then $x = \frac{1}{1837A} = \frac{m_e}{m_p A}$

so since $x \ll 1$ we get

$$\frac{E}{E_0} = 1 - \frac{(1-\cos\theta)}{918A} \quad \text{or} \quad \boxed{\frac{\Delta E}{E_0}(\text{to atom}) = \frac{1-\cos\theta}{918A}}$$

∴ max energy transferred to atom is:

E_{max}

$$\Delta E_{MAX} = \frac{2E_0}{918A} = 4\frac{m_e}{m_p A} \cdot E_0 \; // \quad \text{non-rel. } E_0/mc^2 \ll 1$$

$$\Delta E_{max} = \frac{2m_e}{Am_p} \frac{E_0(E_0 + 2mc^2)}{mc^2} \quad \text{relativistically}$$

kicks in ~50-60 keV //
5% at 50 keV
20% at 100 keV

NOTE / energy transferred to atom depends upon the elec energy (linearly non relativistically)

∴ the recoil energy to the atom is in general.

$$E_{recoil} = E_{max}\left[\sin(\theta/2)\right]^2$$

∴ the critical scatt ∡ which results in atomic displacement of the atom is:

$$\sin(\theta_c/2) = \sqrt{\frac{E_{DISP}}{E_{MAX}}}$$

energy to displace atom

ie if $E_{recoil} > E_{DISPL}$ the atom gets displaced

∴ we can get the "cross section" for displacement

$$\sigma_{DISP} = \int_{\theta_c}^{\pi} \frac{d\sigma_{EL}}{d\Omega} 2\pi \sin\theta \, d\theta$$

$$P_{DISP} = n\sigma_D T$$

density, thickness

and going back, we can get the threshold energy for an inc. electron to displace an atom bound by E_D //

$$E_{Threshold} = m_e c^2\left[\left(1 + \frac{A m_p}{2 m_e}\frac{E_{disp}}{m_e c^2}\right)^{1/2} - 1\right]$$

rel. correct

look at plots as to what this means for KO damage by electrons / steep threshold then relatively constant with energy //

ting
2d
)
)
/
EL

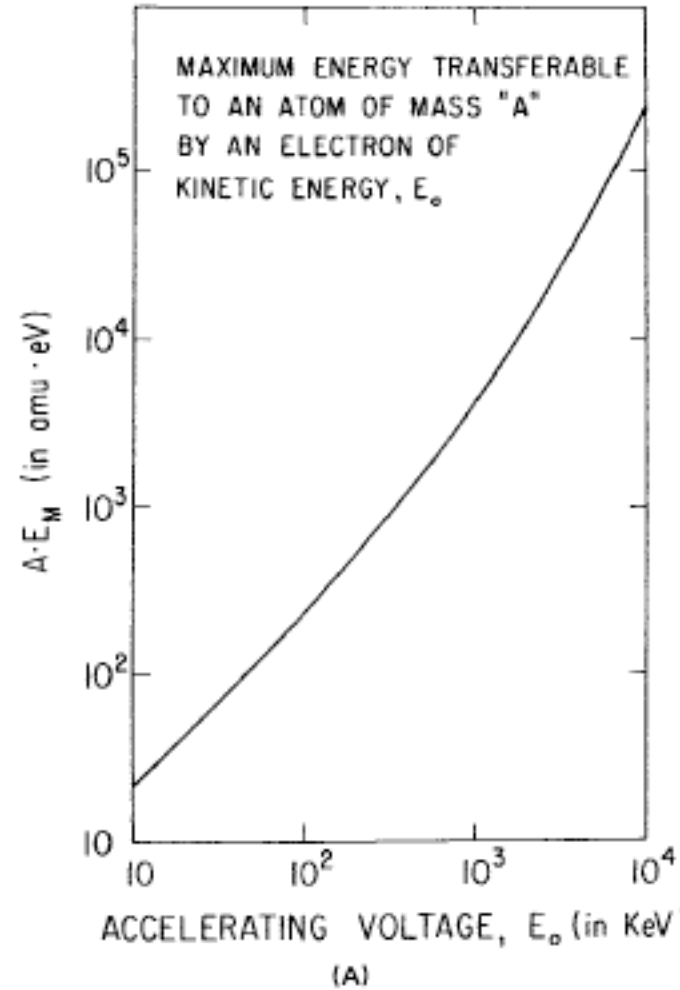

rel. correct

Fig. 1.2 A. The maximum energy which can be transferred by an incident electron of kinetic energy E_0, in an elastic nuclear collision with an atom of mass A. $E_{max} = 2(m/m_pA) \cdot E_0(E_0 + 2mc^2)/mc^2$, where m is the electron rest mass, m_p is the proton rest mass and c is the velocity of light ($M_A = m_p \cdot A$). B. The threshold energy of the incident electron, E_t, necessary just to produce a displacement of an atom of mass A in an elastic nuclear collision. The term E_t is that energy such that the maximum transferable energy shown in Fig. 1.2A is equal to the displacement energy, E_d. The arrows indicate the threshold energies for various atoms assuming $E_d = 1$ eV.

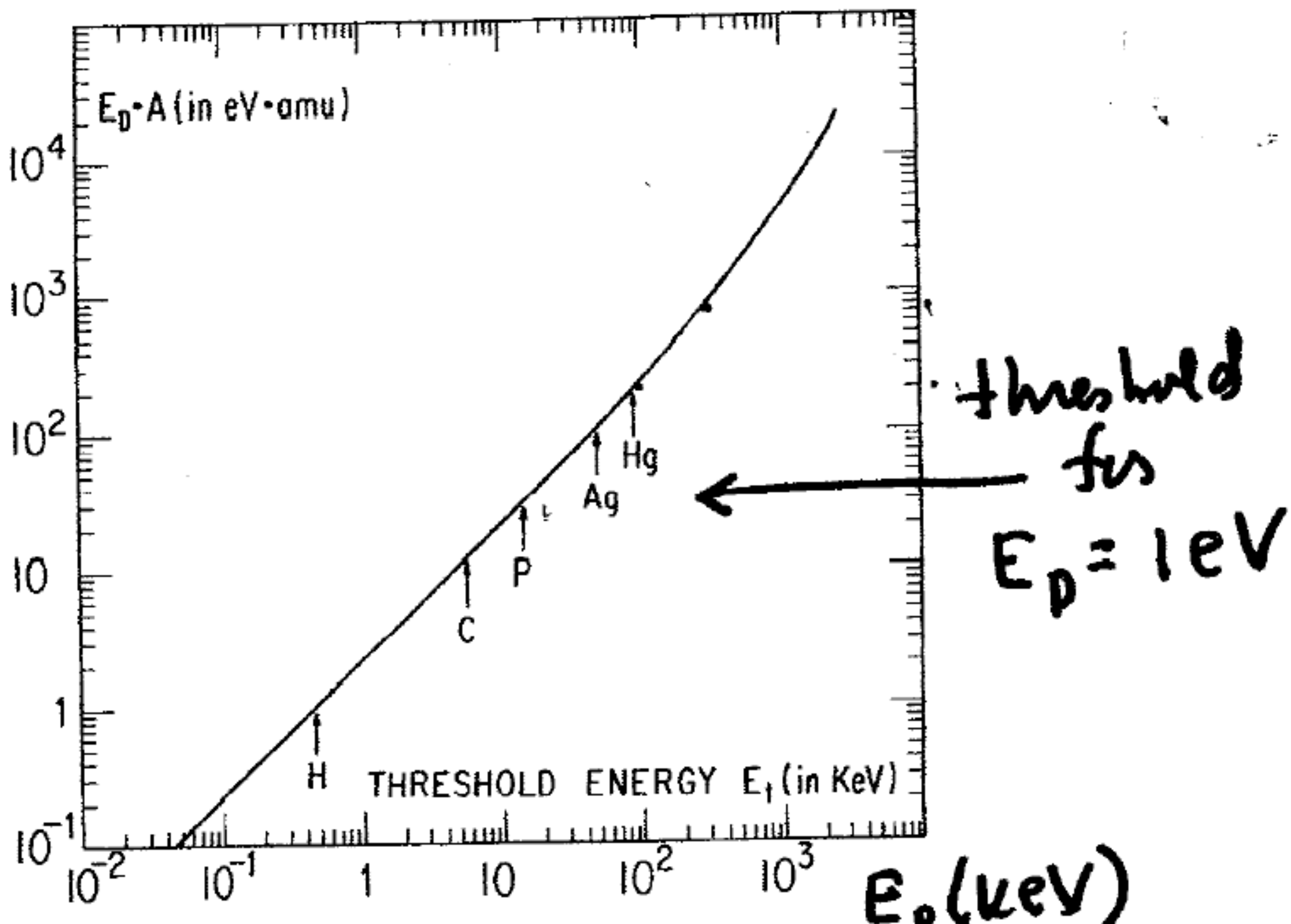

(B)

Fig. 1.2 *(Continued)*

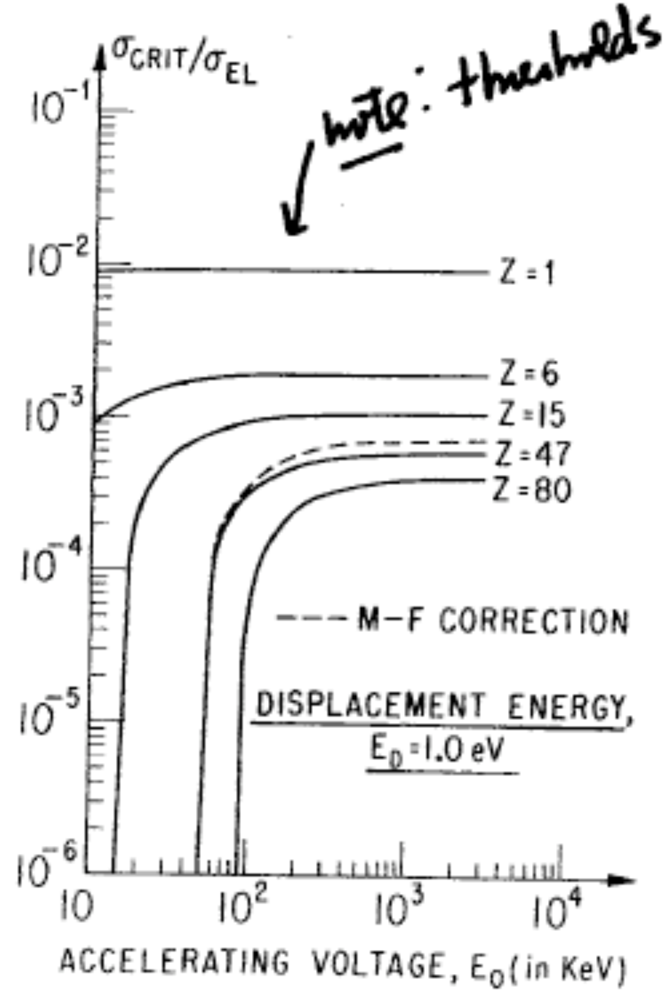

(B)

Fig. 1.3 *(Continued)*

Isaacson, "specimen damage in the electron microscope" in Principles and techniques of electron Microscopy. Vol.8 (ed. M.A. Hayatt.p1-78 (1970). Van Nostrand-Reinhold, NY

(7)

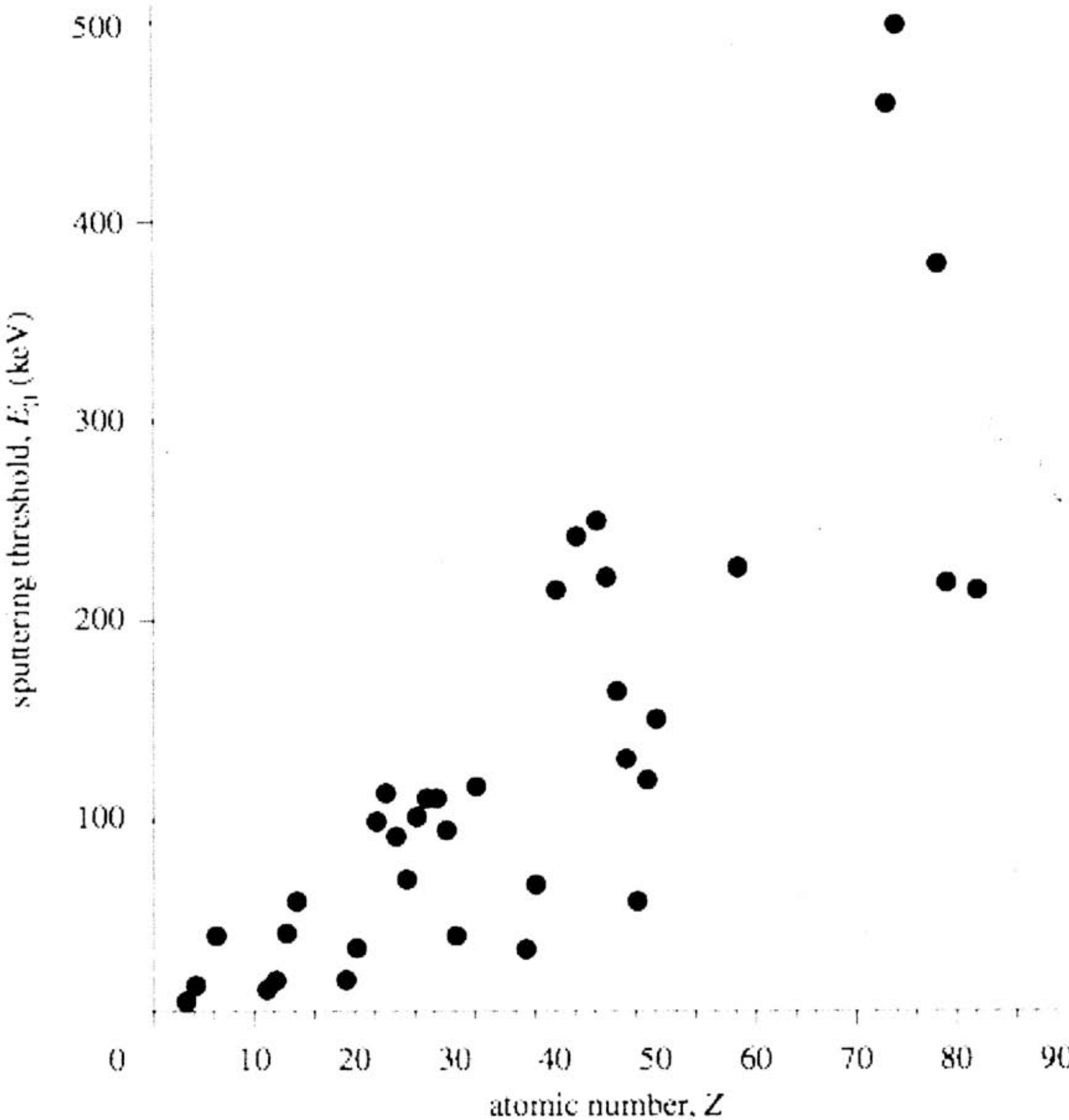

igure 1. Dependence of sputtering threshold on the atomic number (Hobbs 1987).

there is other types of "damage" due to "inelastic events
ie, ionizations events, where we lose electrons from the atoms thereby breaking or altering bonds.

2. "inelastic"

in this case, if there is an energy loss (in the e-e collision) > bond energy, we can break a bond.

this tends to be more prominent for low Z materials / but probability decreases as energy goes up

since $\sigma_{in} \propto \frac{1}{E_0}$ non rel.

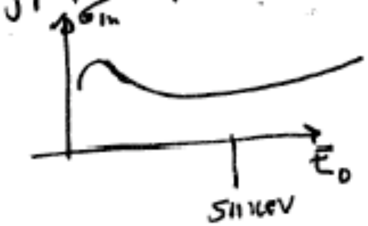

in fact when $E_0 < E_{thresh.}$ for KO displacement
inel. scatt is dominant mechanism for damage.

— look at how damage manifests itself.

ASIDE/ when discussing damage by charged particles we talk about a "dose" which is a "charge density" in charge/unit area.

ie, $J\tau = D$

J = current density, τ = time

$$1 \text{ coul/cm}^2 = 625 \text{ elec/Å}^2$$

(9)

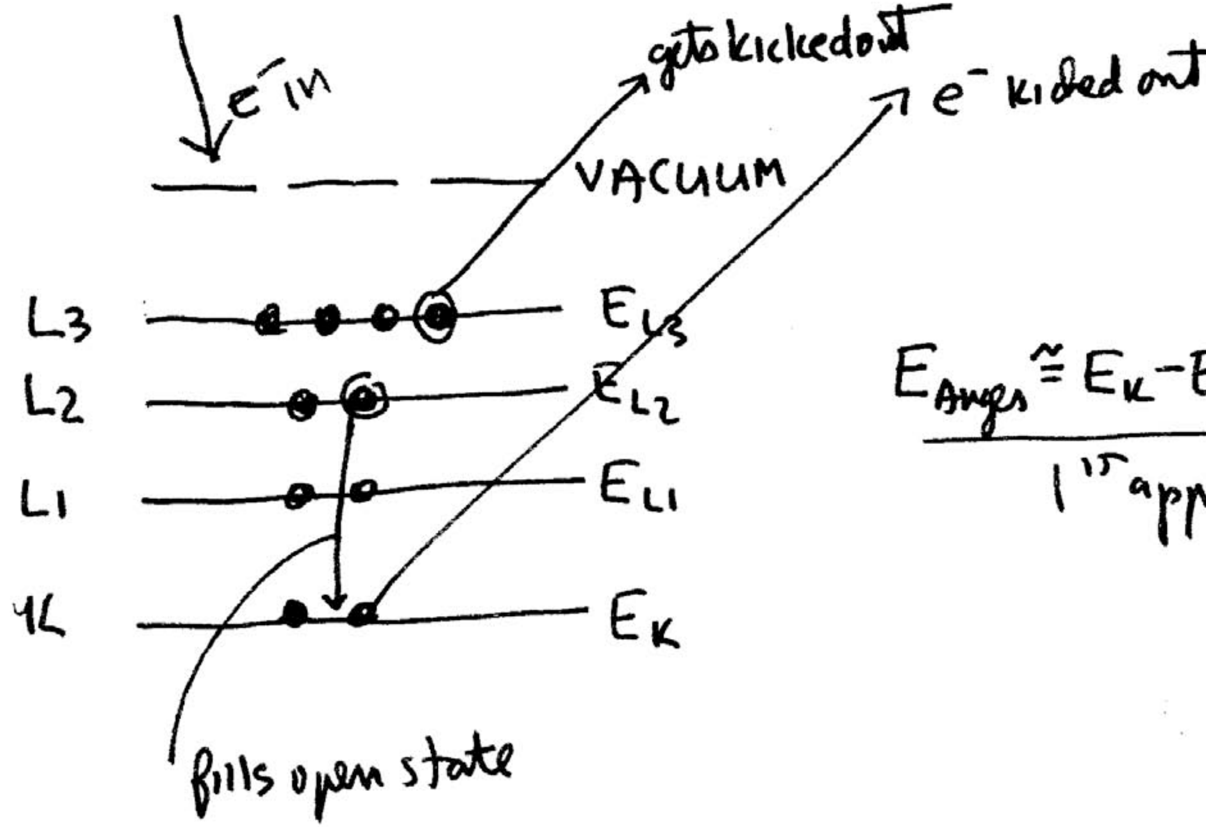

$$E_{Auger} \cong E_K - E_{L2} - E_{L3}$$

1st approx

|| violent rearrangement of electron cloud
can transfer energy to atom → gets displaced

KO then ionization

example, Rohrlich and Carlson, 1954) is within a few percent of that given in Eq. (1.18). So it makes little difference with regard to the energy dependence of damage whether one compares experiments with stopping power calculations or the inelastic scattering cross sections.

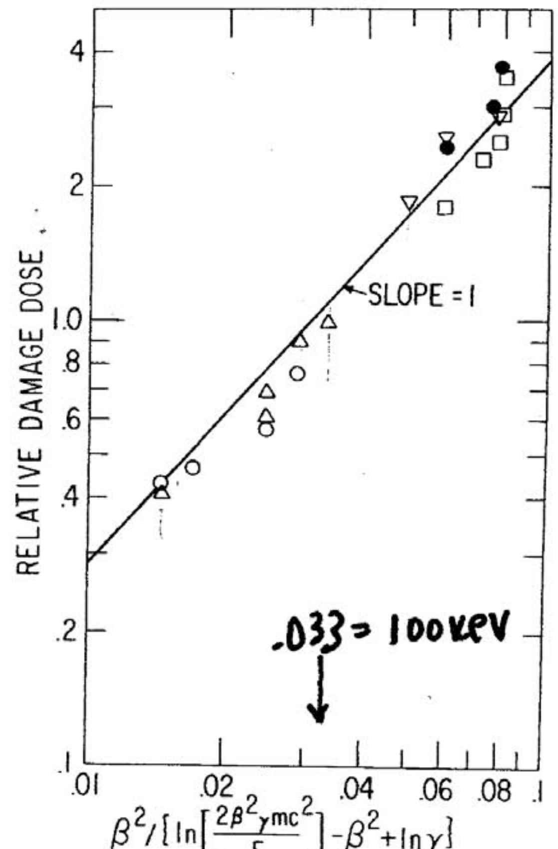

Fig. 1.12 The energy dependence of electron beam damage. The relative damage dose is

$\gamma = \frac{1}{\sqrt{1-\beta^2}}, \beta = \frac{v}{c}$

organic materials

Isaacson, 1970

before looking at different "forms" of damage.
look at signals needed to collect information

$$\underline{S = N J \sigma Y F}$$ signal rate

count for time τ, then

$$S\tau = N(J\tau)\sigma Y F$$

($J\tau$) the "dose" D //

∴ dose delivered is

$$\boxed{D = \frac{S\tau}{N\sigma Y F}}$$

F — efficiency
σ — cross section for event "detected"
N — # contributing to signal

∴ if $(S\tau)_{min}$ is the min. # cts we need to detect a signal ~~over a~~ over a bkg then

the min. dose we can use is

$$D_{min} = \frac{(S\tau)_{min}}{N\sigma Y F} < D_{DAMAGE}$$

if we don't want to "destroy" the object

∴ the fewer atoms/molecules detected, the higher the dose needed to detect them //

Table 1
Electron beam irradiation damage [a]: $E_0 = 100$ keV, room temperature

Observation	Dose (electrons/Å^2)	Material
Diffraction	<1	Nitrocellulose
	$1-10$	Aliphatics
	10^2-10^4	Aromatics
	$1-10^6$	Metal halides
Mass loss	$1-10^3$	Organics
	$1-10^6$	Metal halides
	$10-10^6$	Fluorine desorption
	10^3-10^9	Oxygen desorption
EELS change	10^{-1}	PMMA
	≈ 10	Aliphatics
	$1-10^3$	Metal halides
	10^3-10^{10}	Oxides

[a] Data from this table come from the reviews in refs. [2,3], as well as from other articles in the literature (e.g., refs. [4,6,10,11,13,18]). The doses have been scaled to correspond to an incident electron energy of 100 keV. I have not listed dose rate or ambient conditions, since in most cases these were not reported.

look at a typical organic material damage. L-hist / amino acid.

- xtallinity / $D_{1/e}$ = ~~[illegible]~~ .5 elec/Å^2
- mass / $D_{1/e} \cong$ 5 elec/Å^2
- energy loss (aromatic ring) $D_{1/e}$ = 23 elec/Å^2 | (25 keV)

whereas for non organic materials
the doses may be many orders of mag. greater.
eg atom imaging conditions could result in
$J \sim \frac{1}{2} \times 10^{-10}$ amps/Å^2 sec
$\sim 3 \times 10^{8}$ elec/sec Å^2 →
with 4 μsec/pixel ⟶ 1200 elec/Å^2 ||
and still see no "evidence" of damage.

~

moreover there may be dose-rate effects; ie not total dose but rate is more important! — see example LiF

| sometimes damage correlated with
"ionization" damage (which can result in equiv to sputtering?)
or direct knockons ||

show Auger curve

damage is very material dependent —
if KO damage is a problem ⟹ image at lower inc. energies

1ST lets look at the "doses" for damage
2ND lets see how to reduce that effect.

1. different "types" of e beam induced damage.
   - loss of crystallinity (long range order) -
   - loss of mass (ie, sputtering by KO or ionization)
   - local structural disorder -

each one has a different characteristic
   or rather how the damage proceeds with increasing dose
   - in a single hit model (ie, one event damages)
     the damage is an exponential decay with dose
     ie $\frac{I(t)}{I_0} = e^{-D/D_{1/e}}$, where $D = Jt$
   - if more than one event is required to damage,
     there would be a "latent" dose

show pix

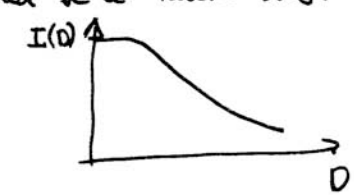

   - - in literature, sometimes one refers to "end pt" dose, D_{ep}
     where D_{ep} would be $(2-5) \times D_{1/e}$ -
     the main pt is $D_{ep} > D_{1/e} > D_{latent}$
   - D's can vary by orders of magnitude
     next

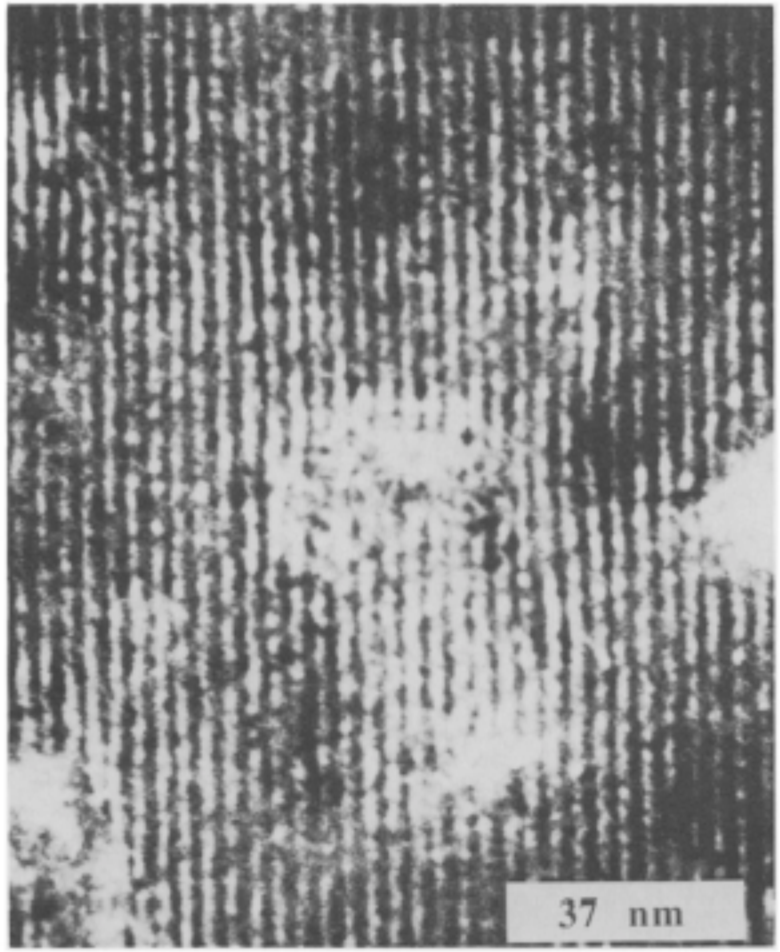

Fig. 1. An example of a grating structure directly etched into lithium fluoride by a 100 keV electron beam using a dose of 10^{-2} C/cm^2. The dose rate was about 5×10^5 A/cm^2, the sample was at 30°C and the vacuum in the sample chamber was 8×10^{-10} Torr. The grating periodicity is 3.7 nm. Such a structure cannot be produced with dose rates less than 10^4 A/cm^2.

reduction of damage

show example

1. spatial averaging methods
   - ie, correlation techniques to "average" individual structures
   - xtal structures whereby you record image & diff. pattern
     - giving you mag and phase.
       (can use many images).

NOTE:
for bio structures
usually need
dose < 5-10 e/Å²

2. cryotemps.
   - slow down thermal motion
   - prevent vaporization
   - frozen in place

   | variable effects

3. "protectants"
   (for biological samples)

4. lower the energy of inc. beam
   — if KO is a problem
   a balancing act between
   KO and ionization //

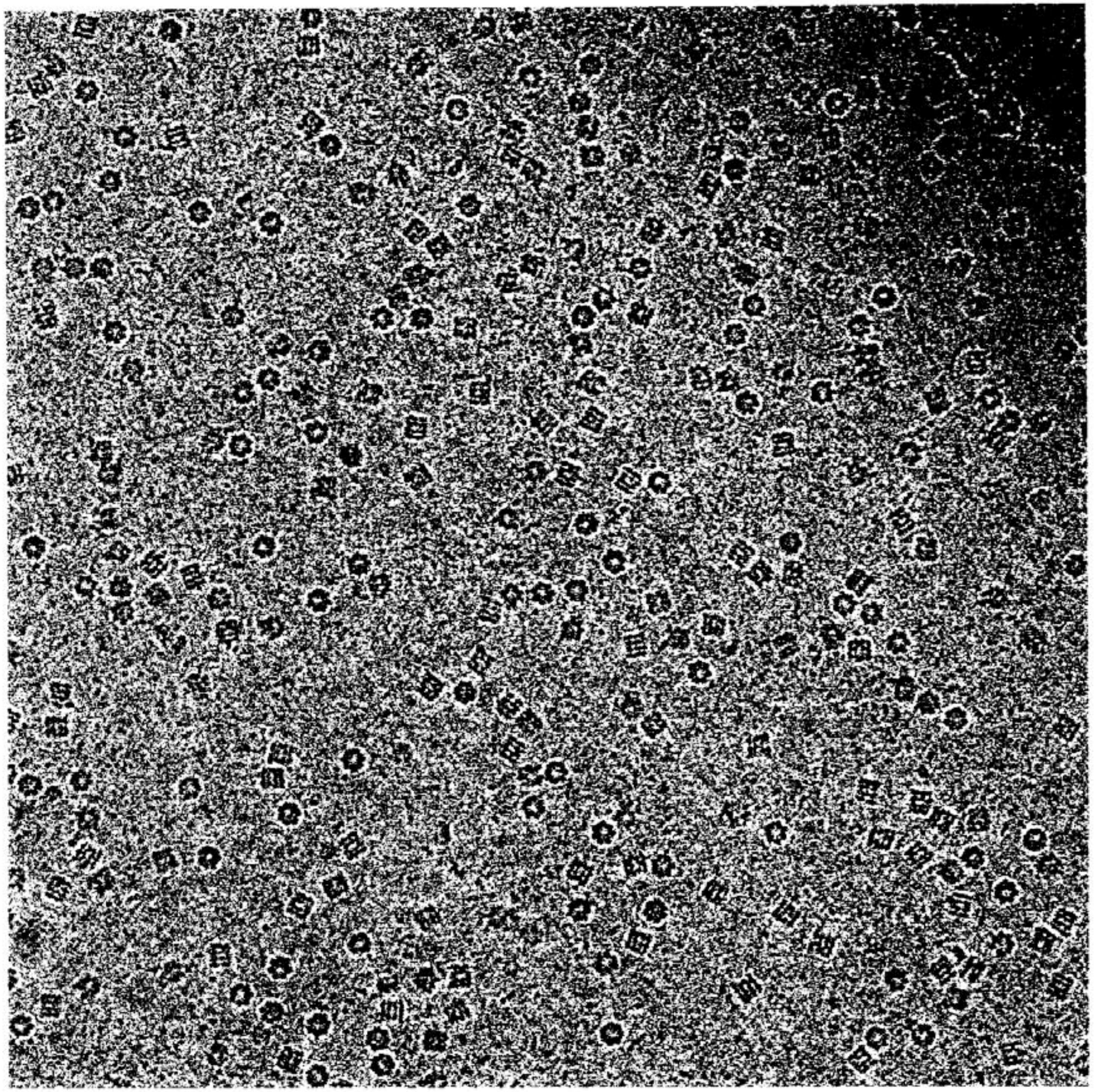

in vitreous ice
at cryotemps

GroEL / a chaperonin – found in bacteria

Vossmann, 2008

size ~ order 15nm/

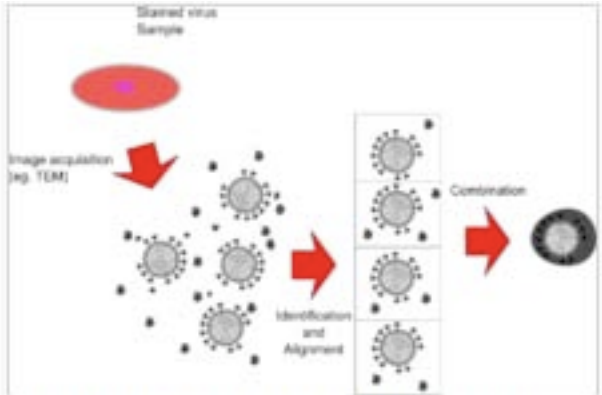

Single particle analysis segments and averages many particles from a sample, allowing for computer algoirthms to process the individual images into a combined "representative" image. This allows for improvements in signal to noise, and can be combined with deconvolution to provide limited improvements to spatial resolution in the image.

- van Heel M, Gowen B, Matadeen R, Orlova EV, Finn R, Pape T, Cohen D, Stark H, Schmidt R, Schatz M, Patwardhan A (200
"Single-particle electron cryo-microscopy: towards atomic resolution.". *Q Rev Biophys*. **33**: 307–69.

Tomographic reconstruction

20

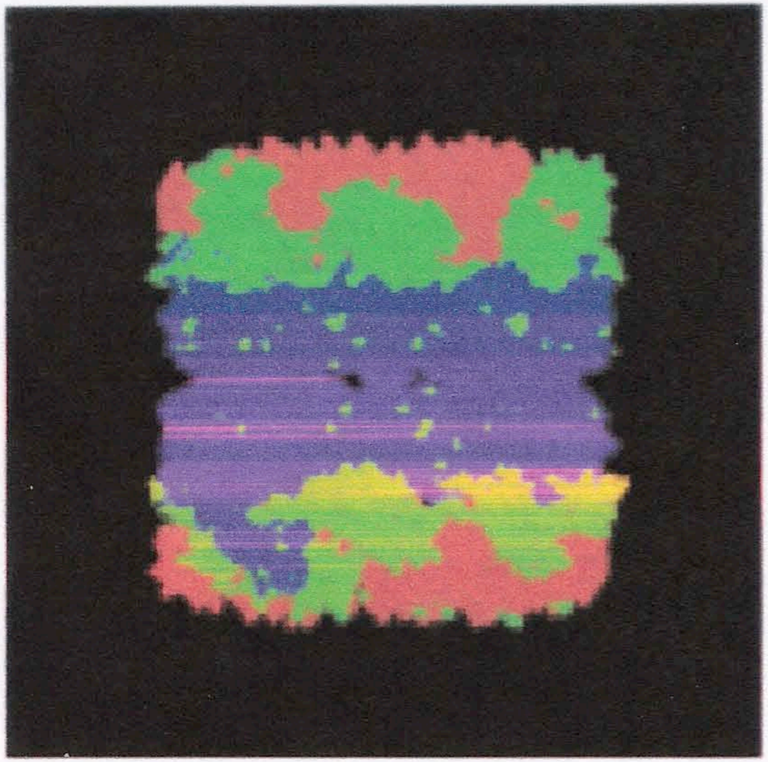

GroEL (side)

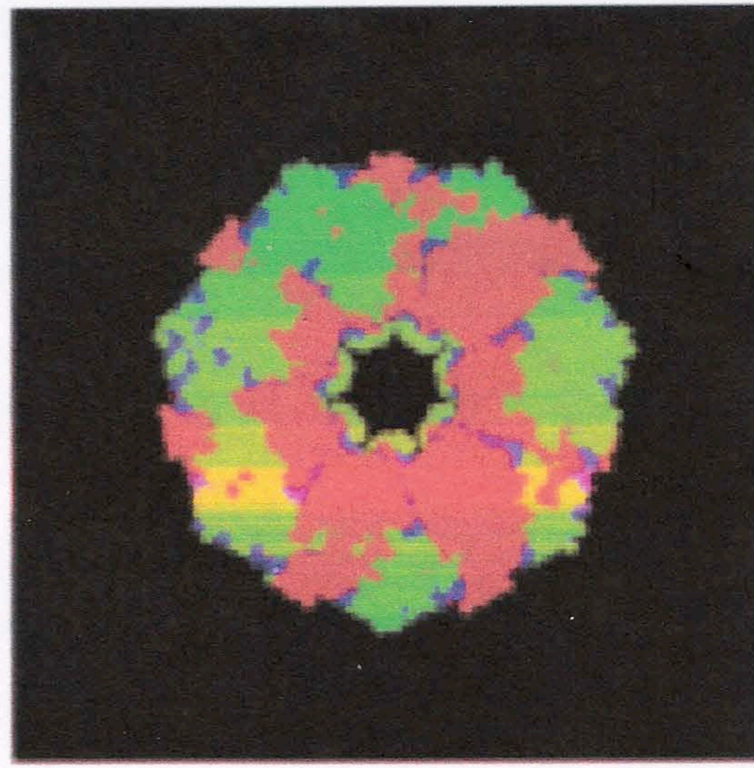

GroEL (top)

← ~15nm →